Title	Multichannel EEG compression : wavelet-based image and volumetric coding approach
Author(s)	Srinivasan, K.; Dauwels, Justin; Reddy, M. Ramasubba
Citation	Srinivasan, K., Dauwels, J., & Reddy, M. R. (2013). Multichannel EEG compression : wavelet-based image and volumetric coding approach. IEEE journal of biomedical and health informatics, 17(1), 113-120.
Date	2012
URL	http://hdl.handle.net/10220/18349
Rights	© 2012 IEEE. This is the author created version of a work that has been peer reviewed and accepted for publication by IEEE Journal of Biomedical and Health informatics, IEEE. It incorporates referee's comments but changes resulting from the publishing process, such as copyediting, structural formatting, may not be reflected in this document. The published version is available at: [DOI:http://dx.doi.org/10.1109/TITB.2012.2194298].

Multichannel EEG compression: Wavelet-based image and volumetric coding approach

K Srinivasan, *Member, IEEE,* Justin Dauwels[†], *Member, IEEE,* M Ramasubba Reddy

Abstract—In this paper, lossless and near-lossless compression algorithms for multichannel electroencephalogram signals (EEG) are presented based on image and volumetric coding. Multichannel EEG signals have significant correlation among spatially adjacent channels; moreover, EEG signals are also correlated across time. Suitable representations are proposed to utilize those correlations effectively. In particular, multichannel EEG is represented either in the form of image (matrix) or volumetric data (tensor), next a wavelet transform is applied to those EEG representations. The compression algorithms are designed following the principle of "lossy plus residual coding", consisting of a wavelet-based lossy coding layer followed by arithmetic coding on the residual. Such approach guarantees a specifiable maximum error between original and reconstructed signals. The compression algorithms are applied to three different EEG datasets, each with different sampling rate and resolution. The proposed multichannel compression algorithms achieve attractive compression ratios compared to algorithms that compress individual channels separately.

Index Terms—arithmetic coding, electroencephalogram (EEG), compression, multichannel EEG, set partitioning coding

I. Introduction

Electroencephalogram (EEG) is a recording of the electrical activity of the human brain, usually acquired by a number of electrodes placed on the scalp. EEG represents brain activity, and much research has been devoted to extracting useful information from EEG. In the past decade, there has been tremendous growth in EEG based research activities, *e.g.,* automated EEG analysis for diagnosis of neurological diseases, and brain computer interfacing (BCI) [1]. In most applications, EEG is recorded from multiple channels (e.g., 64, 128, or 256) and at relatively high sampling frequencies (e.g., few hundred to few thousand Hz). Some applications require storage and/or transmission of EEG recordings over an extended period of time. As a result, EEG recordings may lead to a large amount of data. To efficiently manage storage and/or transmission of EEG signals, we need flexible and efficient compression algorithms.

EEG compression can be classified into two major categories: lossy and lossless compression. The former discards some components of the EEG, and therefore, compresses the EEG substantially, whereas the latter allows perfect reconstruction of the EEG, and as a consequence, only modestly compresses the EEG. In clinical practice, exact reconstruction

K Srinivasan and M Ramasubba Reddy are with Biomedical Engineering Group, Department of Applied Mechanics, IIT Madras, Chennai-600036, India. e-mail: srinivasan.sivam@gmail.com

[†]Corresponding author. Justin Dauwels is with School of Electrical & Electronic Engineering, Nanyang Technological University, Singapore-639798. Singapore. e-mail:jdauwels@ntu.edu.sg

of EEG is more critical than compression performance. In other applications, lossy compression may be more suitable. An attractive compromise between lossless and lossy compression is "near-lossless" compression: relatively high compression rates can be achieved with tolerable distortion, to ensure sufficient accuracy for specific purposes.

In "near-lossless" compression, no sample in the reconstructed signal is changed in magnitude more than δ compared with the original sample, where δ is a nonnegative integer. Let us consider a signal of length N represented by $x = (x(1), x(2), \ldots, x(N))$, and the reconstructed signal (after compression) by $\tilde{x} = (\tilde{x}(1), \tilde{x}(2), \ldots, \tilde{x}(N))$. Near-lossless compression algorithms guarantee the following relationship,

$$||x - \tilde{x}||_\infty = \max_{0 \leq i < N} |x(i) - \tilde{x}(i)| \leq \delta, \qquad (1)$$

where δ is the error tolerance in terms of the number of quantization levels. The distortion measure in eq. (1) is also known as L^∞-norm. The near-lossless compression algorithms proposed in this paper guarantee eq. (1) for a given δ.

EEG signals are typically analyzed in two ways: 1) visual inspection by human experts, 2) automatic analysis using signal processing algorithms. Consequently, any type of compression technique would be suitable as long as the reconstructed EEG signals do not introduce any errors in such analysis. Particularly, near-lossless compression techniques are of great use, as they can limit the distortion to a user defined maximum amount.

Many excellent compression techniques for single-channel EEG compression have been reported so far, which can be categorized under lossless [2]–[5], near-lossless [6, 7] and lossy methods [8]–[13]. Prediction-based coders are very competitive in lossless [4] and near-lossless scenarios [6, 7], when the δ is small (typically 1 or 2). However, none of the aforementioned predictive coding techniques supports progressive transmission. Hence, in many practical scenarios where progressive reconstruction is necessary, they are of limited utility. It is very desirable to combine the advantages of progressive transmission along with the guaranteed maximum distortion in L^∞ sense. However, none of those methods provide guarantees for the maximum distortion. Moreover, all those methods compress each EEG signal separately, whereas one could exploit the correlation among EEG signals from nearby channels. Indeed, EEG signals from adjacent channels are often strongly correlated (inter-channel correlation), and each individual channel has temporal correlations (intra-channel correlation) also.

There are few compression schemes in the literature ad-

dressing multichannel EEG compression; they can be categorized into lossless [5, 14] and lossy [15, 16] methods. All those schemes consider inter- and intra-channel correlation separately, and exploit them by different means. Moreover, as the single-channel methods, they do not allow progressive transmission nor do they provide bounds on the maximum distortion.

In this paper, we propose compression schemes for multichannel EEG that alleviate some of those shortcomings. In particular, our algorithms have the following properties:

- they exploit the inter- and intra-channel correlation simultaneously, by arranging the multichannel EEG as matrix (image) or tensor (volume).
- they support progressive transmission.
- they guarantees a maximum amount of distortion in L^∞ sense, by means of a two-stage coding procedure.

Our algorithms consist of two stages: first the multichannel is arranged as matrix or tensor, which is then subjected to lossy compression using wavelet-based coder; next the residual of the lossy reconstructed data is quantized and compressed in a lossless fashion; this second step allows us to bound the distortion on the residual, and hence also the reconstructed EEG data. We will illustrate this scheme for three distinct EEG datasets, and will provide promising numerical results.

The paper is organized as follows. Section II explains formation of matrix (image) and tensor (volume) from multichannel EEG. Section III describes the two-stage compression algorithm. EEG datasets are elaborated in Section IV, and the performance measures used to analyze the compression algorithms are given in Section V. Results and discussion is presented in Section VI and concluding remarks is given in Section VII.
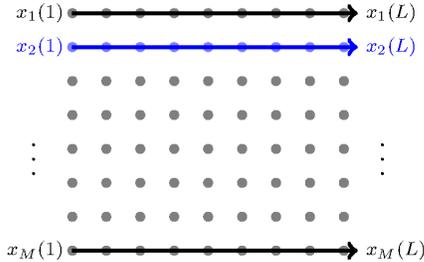

Fig. 1.   2D Image formation from multichannel EEG. The EEG signals from different channels are arranged as rows of the matrix $\mathbf{X}$. The EEG signal from channel i is denoted as x_i.

II. ARRANGEMENT OF MULTICHANNEL EEG IN THE FORM OF 2D IMAGES AND 3D VOLUMES

Spatially adjacent channels of multichannel EEG are strongly correlated, and each individual channel is strongly correlated across time. The multichannel compression schemes proposed so far considered the spatial and the temporal correlation independently and applied different methods to exploit those correlations [5, 14]–[16]. Here, we exploit both spatial and temporal correlations simultaneously in a single procedure. In particular, we arrange multichannel EEG in the form of a 2D image or 3D volume, and next we apply a 2D or
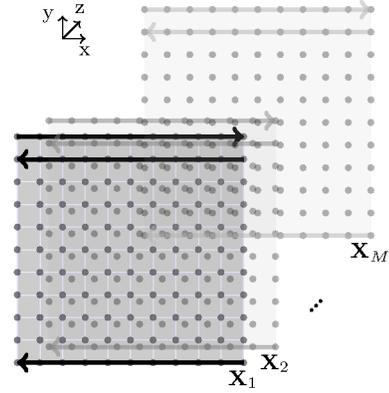

Fig. 2.   Formation of t/dt/s volume from multichannel EEG. The matrices $(\mathbf{X}_1, \dots, \mathbf{X}_M)$ formed from single channel EEG are stacked to form volumetric data. Matrix formation from single-channel EEG is shown (in thick line) for the first slice (signal $x_1(\cdot)$). The signal is divided in segments of length N. The first segment, $x_1(1)$ to $x_1(N)$, is arranged from left to right as the first row, the second segment, $x_1(N+1)$ to $x_1(2N)$, is arranged from right to left as the second row, etc.

3D wavelet transform. In the following sections, we explain how to arrange a multichannel EEG in the form of a 2D image and 3D volumetric data.

A. 2D Image formation from multichannel EEG

Figure 1 shows the formation of 2D image (matrix) from multichannel EEG. The EEG signals from different channels are arranged as rows to form a matrix $\mathbf{X}$. EEG electrode channels are scanned in a spiral fashion [14] for locating adjacent channels. Particularly, adjacent EEG channels are arranged as adjacent rows:

$$
\begin{aligned}
\mathbf{X} &= \{\mathbf{x}_i(t) | i = 1, \dots, M; t = 1, \dots, L\} \quad (2)\\
&= \begin{bmatrix}
x_1(1) & x_1(2) & \cdots & x_1(L) \\
x_2(1) & x_2(2) & \cdots & x_2(L) \\
\vdots & \vdots & \ddots & \vdots \\
x_M(1) & x_M(2) & \cdots & x_M(L)
\end{bmatrix}_{(M \times L)}.
\end{aligned}
$$

Adjacent EEG channels are typically substantially correlated. Therefore, the 2D image represented by matrix $\mathbf{X}$ is typically locally smooth: each entry of $\mathbf{X}$ is similar compared to its immediate row and column neighbors. However, the correlation decreases as one moves farther along the rows or columns.

B. 3D volume formation from multichannel EEG

We consider two ways to extract a 3D tensor from multichannel EEG signals. The first approach is illustrated in Fig. 2. In [17], we arranged single-channel EEG in matrix form before compression, and this resulted in improved lossless compression compared to conventional vector form compression. Here, we arrange single-channel EEG in matrix form, and the matrices associated with the single-channel EEG signals are stacked to form 3D volume (tensor), as depicted in Fig. 2. Adjacent slices in the tensor correspond to adjacent EEG channels; we accomplish this by scanning the electrodes in a spiral fashion [14]. We refer to this volume as "t/dt/s", where
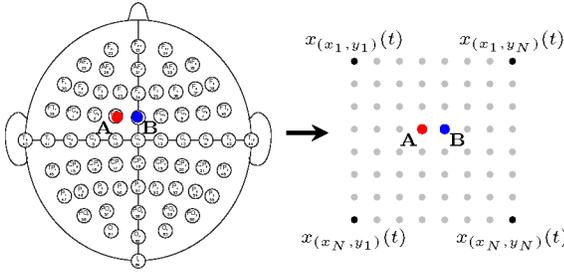
Fig. 3. Formation of matrix from multichannel EEG signals. 64-channel EEG montage is shown on the left. At a particular time instance t, the samples from all the channels are arranged in the form of matrix, as shown on the right. The adjacent entries in the matrix stem mostly from spatially adjacent channels. For example, the spatially adjacent channels (A and B) correspond to adjacent entries in the matrix.
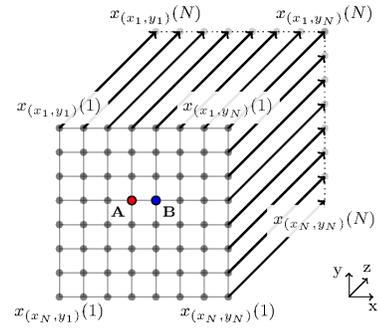

Fig. 4. Formation of s/s/t volume. At any time instance, we form matrix from the multichannel EEG, as shown in Fig. 3. N such matrices formed at subsequent time instances are then stacked along the z-direction to form a volume.

the x, y, and z directions reflect temporal (t), delayed temporal (dt), and spatial (s) variations respectively. The k-th slice of the volume $\mathcal{X}_{t/dt/s}$, denoted by $\mathbf{X}_k$, can be written as:

$$\mathcal{X}_{t/dt/s}^{(k)} = \{\mathbf{X}_k | k = 1, \ldots, M\}, \tag{3}$$

$$= \begin{bmatrix} x_k(1) & x_k(2) & \cdots & x_k(N) \\ x_k(2N) & x_k(2N-1) & \cdots & x_k(N+1) \\ \vdots & \vdots & \ddots & \vdots \\ \cdot & \cdot & \cdots & x_k(N^2) \end{bmatrix}_{(N \times N)}.$$

We also consider an alternative and simple method to form a tensor from multichannel EEG. A matrix is formed from the multichannel EEG at each time instance (see Fig. 3); the matrices formed at subsequent time instances are stacked to form a volume, as depicted in Fig. 4. Since EEG signals from spatially adjacent channels have significant correlation, we form matrices with similar adjacency as the EEG montage. We call this volumetric data as "s/s/t", because $x-y$ plane reflects the spatial correlations, and the temporal correlations can be found along the z direction. The k-th slice of the volume may be written as:

$$\mathcal{X}_{s/s/t}^{(k)} = \{x_{(i,j)}(k) | i = 1, \ldots, N_1, j = 1, \ldots, N_2\} \tag{4}$$

$$= \begin{bmatrix} x_{(1,1)}(k) & x_{(1,2)}(k) & \cdots & x_{(1,N_2)}(k) \\ x_{(2,1)}(k) & x_{(2,2)}(k) & \cdots & x_{(2,N_2)}(k) \\ \vdots & \vdots & \ddots & \vdots \\ x_{(N_1,1)}(k) & x_{(N_1,2)}(k) & \cdots & x_{(N_1,N_2)}(k) \end{bmatrix}_{(N_1 \times N_2)},$$

where i and j refer to the position in the x-y plane, whereas the slice number k refers to the time index. The dimension of the $x-y$ plane is limited by the number of channels. The slices in the $x-y$ plane may be square or rectangular.

III. TWO-STAGE NEAR-LOSSLESS CODER

Figure 5 shows a diagram of the proposed two-stage near-lossless coder for multichannel EEG. We denote the EEG in matrix or tensor form by I. At encoder side, in the first stage, we compress I by means of a scalable wavelet encoder based on successive bit-plane encoding, resulting in the compressed data I_{en}; we use bi-orthogonal wavelet transform (5/3 filters) as in our previous work [2]. The compressed data I_{en} is then decoded to give lossy approximation I_l of the original data I.

Next we quantize the residue $\varepsilon = I - I_l$, resulting in ε_q, which in turn is compressed by residual coding, leading to ε_{q-en}. At the decoder end, both I_{en} and ε_{q-en} are used to obtain the near-lossless reconstruction I_{nl} of I. As illustrated in Fig. 5(b), I_{nl} is obtained by combining the lossy reconstruction I_l and the dequantized residual $\hat{\varepsilon}$, i.e., $I_{nl} = I_l + \hat{\varepsilon}$. Finally, I_{nl} is rearranged to yield the near-losslessly reconstructed EEG signal(s). We now discuss the scheme in more detail. We can readily confirm the following relations:

$$I = I_l + \varepsilon, \tag{5}$$
$$I_{nl} = I_l + \hat{\varepsilon}. \tag{6}$$

Therefore, it follows that $||I - I_{nl}||_\infty = ||\varepsilon - \hat{\varepsilon}||_\infty$, and hence $||\varepsilon - \hat{\varepsilon}||_\infty \le \delta$ is equivalent to $||I - I_{nl}||_\infty \le \delta$. The residual ε is uniformly quantized to generate quantization indices ε_q:

$$\varepsilon_q = \begin{cases} \lfloor \frac{\varepsilon+\delta}{2\delta+1} \rfloor, & \varepsilon > 0 \\ \lfloor \frac{\varepsilon-\delta}{2\delta+1} \rfloor, & \varepsilon < 0 \end{cases}, \tag{7}$$

where $\lfloor \cdot \rfloor$ denotes the integer part of the argument. The quantized residual ε_q is then losslessly encoded by residual coding procedure. Hence, I_{en} is transmitted as output of the lossy coding layer, and the losslessly coded quantization index ε_{q-en} is sent as output of the residual coding layer.

At the decoder end, the residual bitstream ε_{q-en} is decoded to yield ε_q followed by a dequantizer, defined as follows, to guarantee $||\varepsilon - \hat{\varepsilon}|| \le \delta$:

$$\hat{\varepsilon} = (2\delta + 1)\varepsilon_q. \tag{8}$$

By adding the lossy reconstruction I_l and the dequantized residual $\hat{\varepsilon}$, we obtain the final near-lossless reconstruction I_{nl} with guarantee $||I - I_{nl}|| \le \delta$.

The formation of image/volume from multichannel EEG, is the principal difference from the coders used for image/volumetric compression [18]; the other steps are very similar.

We used two different wavelet-based lossy encoders in the first stage of the compression algorithm. Wavelet transformation of natural signals yield transform coefficients with close values occurring in clusters. The algorithms used here are based on set partitioning principle [19], where the wavelet coefficients are grouped first into sets, which are then split recursively to locate the significant coefficients at a particular
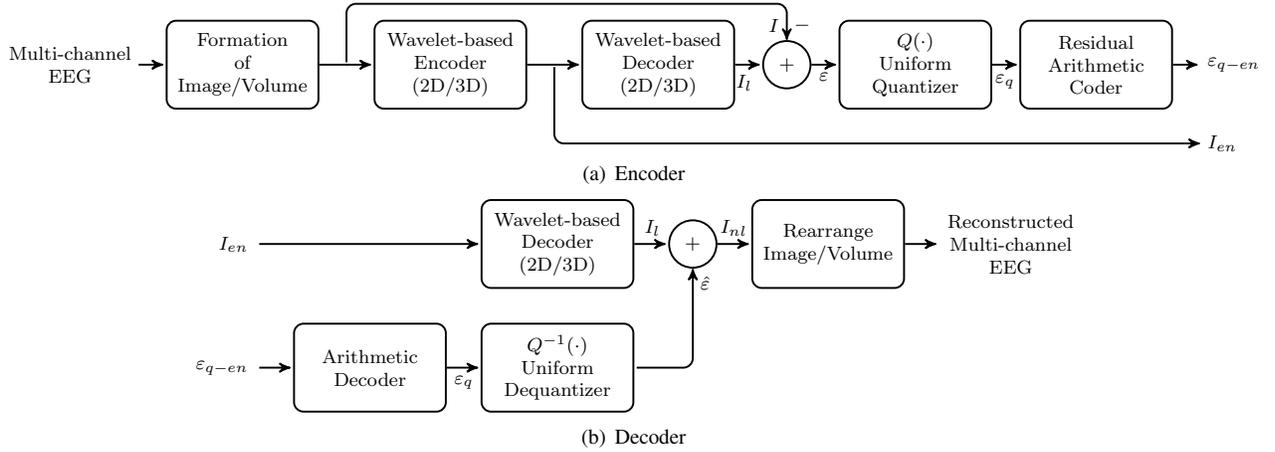
(a) Encoder

(b) Decoder

Fig. 5. Block diagram of the two-stage coder for multichannel EEG.

TABLE I
EEG DATASETS USED FOR TESTING THE ALGORITHMS

Dataset Name	No. of Channels	f_s (Hz)	Resolution (bits)	Total Duration	No. of Subjects
EEG-MMI	64	80	12	24 min	12
BCI3-MI	118	100	16	50 s	5
BCI4-MI	64	1000	16	50 s	5

threshold. We use the following wavelet coders: (i) set partitioning in embedded block (SPECK) [20, 21], and (ii) binary set splitting in k-d trees (BISK) [22, 23]. The above algorithms have the following attributes: (i) progressive quality, (ii) progressive resolution and (iii) bitstream can be truncated at any point below the encoded rate to give the best quality reconstruction at that particular rate.

In the residual arithmetic coding stage, we directly code the residual if the symbol size N is small ($N \leq 128$). In some cases, the probability distribution of the source is simultaneously peaked and long tailed leading to large symbol size ($N > 128$); direct arithmetic coding of such sequences will be complex due to large symbol size [24]. To reduce complexity, we group symbols together, and each symbol in the residual stream is split into three: 1) sign index: the sign of the symbol, 2) group index: the group which the symbol belongs, and 3) symbol index: the rank of the symbol inside the particular group. The symbol size of these separate index streams will be smaller compared to the original symbol stream, and hence arithmetic coding of the separate symbol stream will be less complex and faster compared to direct arithmetic coding [25].

IV. DATASETS

The compression algorithms are tested using three different EEG datasets. Table I lists important details of the EEG datasets. More details are given in the following paragraphs.

Motor Movement/Imagery Database (EEG-MMI): EEG signals were acquired with 64-channel international 10/10 configuration. The recordings were made in healthy subjects performing motor imagery tasks by the BCI2000 system

[26, 27]. The EEG signals were sampled at $80\,\text{Hz}$ and digitized at $12\,\text{bit}$ resolution. For testing algorithms, 12 recordings are randomly selected from total 109 recordings. In each recording, two one-minute EEGs are considered; these EEGs correspond to subject in idle state with eyes open and closed conditions.

Motor Imagery dataset-II (BCI3-MI): EEG signals were recorded by 128-channel system, where 118 channels were measured exactly at positions of extended international 10/20 configuration [28]. The signals were analog band-pass filtered between 0.05 and $200\,\text{Hz}$, sampled at $1000\,\text{Hz}$ with $16\,\text{bit}$ resolution, and then downsampled to $100\,\text{Hz}$. The recordings were done for healthy volunteers while performing a motor imagery task. A subset of 64 channels is selected for testing compression algorithms.

Motor imagery dataset-I (BCI4-MI): This database consists of 64-channel EEG signals recorded with densely distributed electrodes in sensorimotor areas [29]. The signals were band-pass filtered between 0.05 to $200\,\text{Hz}$ and then sampled at $1000\,\text{Hz}$ and digitized at $16\,\text{bit}$ resolution. EEG signals were recorded when the subject is performing a cued motor imagery task.

V. PERFORMANCE MEASURES

We assess our EEG compression algorithms by three measures: compression ratio, percent root-mean-square distortion (PRD), and peak signal-to-noise ratio (PSNR).

A. Compression Ratio

The compression ratio is the reduction in file size, defined as:

$$CR = \frac{L_{orig}}{L_{comp}}, \tag{9}$$

where L_{orig} and L_{comp} refer to bitstream length of the original and compressed sources respectively.

B. Distortion Measures

The difference between the original and the reconstructed signal is given by $e = x - \tilde{x}$, where x and $\tilde{x}$ refer to original and reconstructed signal respectively. Distortion measures are computed from the error signal e. We consider two distortion measures: percent root-mean-square distortion and peak signal-to-noise ratio. The former quantifies the average distortion, whereas the latter measures the local or worst-case distortion.

1) Percent Root-Mean-square distortion (PRD): The percent root-mean-square distortion (PRD) is given by the following equation,

$$PRD(\%) = \sqrt{\frac{\sum_{i=1}^{N}[x(i)-\tilde{x}(i)]^2}{\sum_{i=1}^{N} x(i)^2}} \times 100,$$

$$= \sqrt{\frac{\sum_i e(i)^2}{\sum_i x(i)^2}} \times 100. \quad (10)$$

The PRD is based on the ratio of energy of the error signal to energy of the original signal. This is a widely used distortion measure and gives the amount of average distortion present in the reconstructed signal.

2) Peak signal-to-noise ratio (PSNR): The maximum absolute error (MAE) between the original signal x and the reconstructed signal $\tilde{x}$ is given by:

$$MAE(x,\tilde{x}) = \max_{0 \leq i < N} |x(i) - \tilde{x}(i)|. \quad (11)$$

Clearly, the MAE depends on the EEG sample having largest error. Consequently, this measure does not provide information regarding the amount of error in the other samples, and hence it is local in nature.

It is not meaningful to directly compare the MAE of EEG signals of different sampling resolution, since the range of the EEG signals differs for different datasets. Therefore, we need to normalize MAE by the signal range leading to distortion measure called as peak-signal-to-noise ratio, which is defined in logarithmic scale (in dB) as follows:

$$PSNR(x,\tilde{x}) = 10 \log_{10} \left(\frac{2^Q - 1}{MAE(x,\tilde{x})} \right) \quad \in [0, \infty]. \quad (12)$$

Interestingly, two different error signals e may have the same value of PSNR but different value of PRD, and vice versa. The PRD quantifies the average distortion, whereas PSNR describes the worst case distortion. To assess the average and worst-case performance of compression algorithms, we need to use PRD alongside with PSNR.

VI. RESULTS AND DISCUSSIONS

We apply our proposed multichannel near-lossless EEG compression algorithm (cf. Fig. 5) to the three datasets mentioned in Section IV. We used a block size of 1024 samples from each EEG channel. For comparison, we also compress single-channel EEGs separately. EEG from each channel is arranged in the form of matrix of size 32×32 before compression, as large matrix sizes led to very little or no improvement in compression [2]. For multichannel case, the
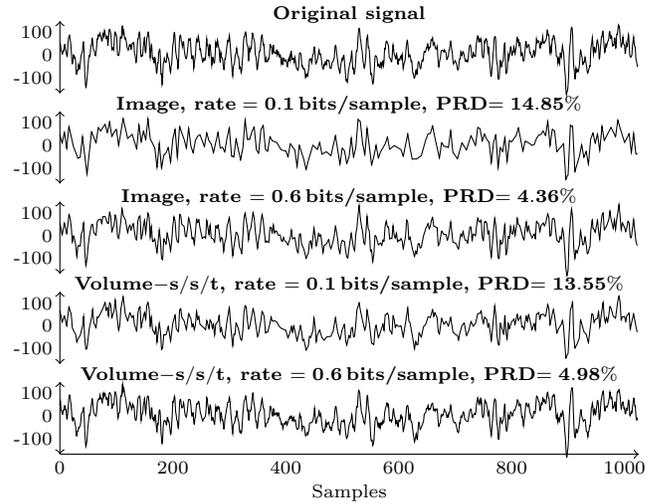

Fig. 6. Progressive reconstruction of EEG signals. Reconstruction for bit-rates of 0.1 bits/sample and 0.6 bits/sample for Image and Volume-s/s/t algorithm are given. Both the algorithms operate with SPECK in the lossy-coding layer.

EEG is arranged either in the form of image or volumetric data as discussed in Section II, before usual compression procedure We use the open-source library QccPack [30] for implementing the compression algorithms.

A. Lossy coding layer and selection of optimal rate

In the two-stage coding procedure, the lossy layer coding is halted at an optimal rate, and the residual is compressed further by residual arithmetic coding after quantization. The optimal rate is the point where the encoding residual of the source becomes i.i.d., and hence lacks the structure that a lossy encoder can take advantage of; hence it is efficient in switching to entropy coder after the optimal rate [2, 18].

The optimal rate is determined empirically. Progressive reconstructions of one channel EEG signal is given in Fig. 6. Most of the prominent signal variations are captured with a bit rate of 0.1 b/s, and a further increase in bit rate to 0.6 b/s captures only minute variations. We use an optimal rate of 1.5 b/s for the lossy coder (for all our algorithms) due to its good performance in our experiments, and also for a fair comparison between the different compression algorithms.

B. Near-lossless multichannel EEG compression

In near-lossless compression, we study the performance by varying step size δ of the quantizer; for each step size, we calculate the compression ratio and the two distortion measures (PRD and PSNR).

In Fig. 7(a), we show how the compression ratio increases with the quantizer step size δ for the EEG-MMI dataset. We also provide the average (PRD) and worst case (PSNR) error with compression ratio in Fig. 7(b) & (c) respectively.

Detailed numerical results for all three EEG datasets are presented in Table II, for single and multichannel compression algorithms, with two different lossy layer coders at three quantization step size values.

The compression ratio for a given step size δ is largest for the EEG dataset (EEG-MMI) with lowest sample frequency
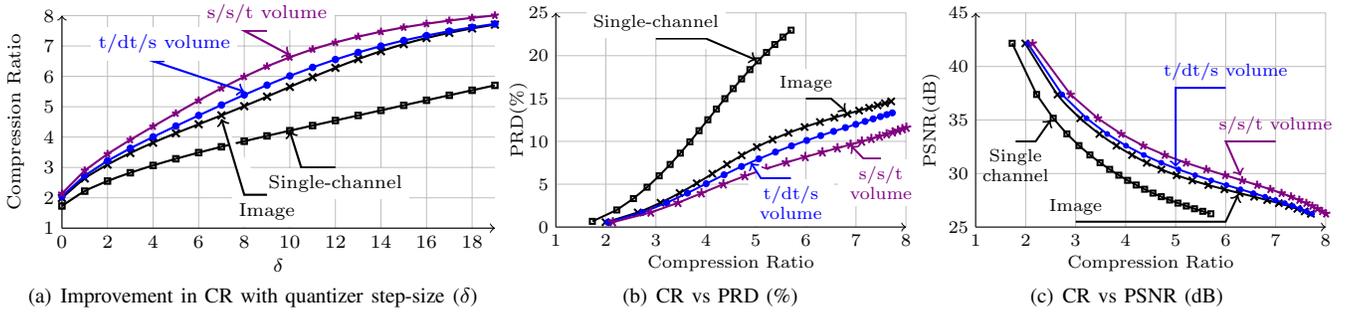
Fig. 7. Performance of single-channel, image and volumetric compression of multichannel EEG. All the algorithms operate with SPECK in lossy coding layer.
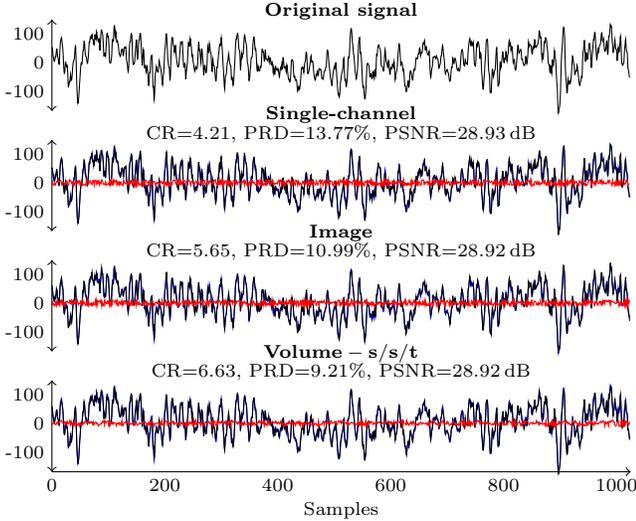

Fig. 8. Original and reconstructed signals for single-channel, Image and Volumetric-based compression schemes; all the algorithms operate with a quantizer step-size $\delta = 10$. The reconstructed signals are superimposed with the original signal in blue. Error between the original and reconstructed signal is superimposed and shown in red for easier comparison. Only a single channel signal is shown here. Y-axis refers to quantization values.

f_s and lowest amplitude resolution, compared to the datasets with higher f_s and resolution (BCI3-MI & BCI4-MI). The PSNR values are higher (and hence the MAE values are lower) for the datasets with higher amplitude resolution, particularly, the PSNR values are higher for BCI3-MI and BCI4-MI (both 16 bit resolution) than for EEG-MMI (12 bit). Likewise, the PRD is lower for BCI3-MI and BCI4-MI than for EEG-MMI. For datasets with higher amplitude resolution, a given step size δ corresponds to smaller error.

As an illustration, we show the original signal and reconstructed signal in Fig. 8, for one channel EEG for single-channel, image and volumetric based compression algorithms (Table II, $\delta = 10$, EEG-MMI). The reconstructed signal closely resembles the original signal, and it is difficult to adjudge the performance of the algorithms by visual inspection of reconstructed and error signals. The error measures, however, are reported in Table II. The best performance in terms of CR, PRD, and PSNR for each data set and δ-value is indicated in bold face. Note that the PRD and PSNR is comparable for each method, for a given dataset and δ value.

Clearly, multichannel EEG compression algorithms achieve larger compression ratios (CR), for a particular value of error δ, compared to single-channel methods. This observation confirms that inter-channel correlations may be exploited to achieve better compression.

Let us now compare volumetric-based with image-based compression algorithms. The s/s/t and t/dt/s volume approach achieve the highest CR for the EEG-MMI and BCI3-MI dataset respectively, both for lossless compression ($\delta = 0$) and near-lossless compression with different tolerance values. Interestingly, for the BCI4-MI dataset, the image-based scheme performs slightly better in terms of CR compared to volumetric schemes. That dataset has much higher sample frequency than the other two datasets. Note that we consider a block size of 1024 samples in each channel. When the sampling rate is low (EEG-MMI and BCI3-MI dataset), each block covers a large time span, and the volumetric based compression schemes are better capable of exploiting long-term correlations than image based methods. However, if the sampling rate is high, the samples within each block cover a short time span, and they are strongly correlated. The image-based methods are capable of exploiting those short-term correlations effectively, and as a result, they perform as well as the volumetric methods (and even slightly better for the BCI4-MI dataset). In summary, the volumetric-based multichannel compression algorithms achieve higher compression than image-based compression algorithms for most EEG data sets, since they utilize the inter-channel correlation effectively.

VII. CONCLUSION

In this paper, we proposed novel compression algorithms for multichannel EEG. We represent the EEG in the form of an image (matrix) or volume (tensor). Such representations help to exploit both the spatial and temporal correlations. We followed a "two-stage" coding philosophy: the EEG data is first coded at an optimal rate using a wavelet-based scheme, and next the residuals are further encoded by an entropy coding scheme (particularly, modified arithmetic coding). We achieve attractive compression ratios for low error values.

REFERENCES

[1] E. Nidermeyer and F. L. D. Silva, *Electroencephalography:Basic Principles, Clinical applications and related fields*, 5th ed. Lippincott Williams and Wilkins, 2005.

[2] K. Srinivasan, J. Dauwels, and M. R. Reddy, "A two-dimensional approach to lossless EEG compression," *Biomed. signal process. and control*, vol. 6, pp. 387–394, 2011.

TABLE II
Lossless/Near-lossless compression performance of single-channel (SC) and multichannel (MC) compression algorithms. multichannel compression include image-based (MC-Image) and volumetric-based (MC-t/dt/s & MC-s/s/t) compression algorithms. Best performing algorithm for the particular case is indicated in bold face.

Lossy Layer coder		SPECK			BISK		
Method	δ	CR	PRD	PSNR	CR	PRD	PSNR
EEG-MMI							
SC		1.73	0.66	42.17	1.74	0.67	42.17
MC-Image	0	1.99	0.57	42.15	1.99	0.57	42.15
MC-t/dt/s		2.04	0.57	42.14	2.06	0.57	42.14
MC-s/s/t		**2.14**	**0.57**	**42.14**	2.10	0.57	42.14
SC		3.28	7.30	31.74	3.31	7.30	31.74
MC-Image	5	4.12	6.22	31.73	4.12	6.22	31.73
MC-t/dt/s		4.36	6.09	31.73	4.42	6.09	31.73
MC-s/s/t		**4.78**	**5.96**	**31.73**	4.60	6.02	31.73
SC		4.21	13.77	28.93	4.24	13.76	28.93
MC-Image	10	5.65	10.99	28.92	5.64	11	28.92
MC-t/dt/s		6.02	10.11	28.92	6.12	9.97	28.92
MC-s/s/t		**6.63**	**9.21**	**28.92**	6.36	9.53	28.92
BCI3-MI							
SC		1.68	0.10	51.23	1.68	0.10	51.23
MC-Image	0	1.75	0.07	51.22	1.75	0.07	51.22
MC-t/dt/s		1.93	0.07	51.18	**1.94**	**0.07**	**51.18**
MC-s/s/t		1.91	0.07	51.18	1.86	0.07	51.18
SC		2.66	1.31	40.77	2.67	1.04	40.77
MC-Image	5	2.84	0.81	40.77	2.84	0.81	40.77
MC-t/dt/s		3.32	0.81	40.76	**3.36**	**0.81**	**40.76**
MC-s/s/t		3.23	0.81	40.76	3.14	0.81	40.76
SC		3.17	1.98	37.96	3.18	1.98	37.96
MC-Image	10	3.40	1.55	37.96	3.40	1.55	37.96
MC-t/dt/s		4.10	1.54	37.95	**4.15**	**1.55**	**37.95**
MC-s/s/t		4.03	1.55	37.95	3.83	1.55	37.95
BCI4-MI							
SC		1.51	0.10	51.30	1.52	0.11	51.30
MC-Image	0	**1.51**	**0.08**	**51.29**	**1.51**	**0.08**	**51.29**
MC-t/dt/s		1.50	0.08	51.18	1.50	0.08	51.18
MC-s/s/t		1.49	0.08	51.18	1.48	0.08	51.18
SC		2.27	1.16	40.77	2.28	1.16	40.78
MC-Image	5	**2.27**	**0.90**	**40.77**	2.27	0.90	40.77
MC-t/dt/s		2.24	0.89	40.76	2.25	0.90	40.76
MC-s/s/t		2.21	0.90	40.76	2.21	0.90	40.76
SC		2.64	2.22	37.96	2.65	2.23	37.97
MC-Image	10	**2.63**	**1.72**	**37.96**	**2.63**	**1.72**	**37.96**
MC-t/dt/s		2.61	1.72	37.95	2.61	1.72	37.95
MC-s/s/t		2.56	1.72	37.95	2.55	1.72	37.95

[3] N. Sriraam and C. Eswaran, "Context based error modeling for lossless compression of EEG signals using neural networks," *J. Med. Syst.*, vol. 30, pp. 439–448, 2006.

[4] ——, "An adaptive error modeling scheme for the lossless compression of EEG signals," *IEEE Trans. Inf. Technol. Biomed.*, vol. 12, no. 5, pp. 587–594, Sep. 2008.

[5] G. Antoniol and P. Tonella, "EEG data compression techniques," *IEEE Trans. Biomed. Eng.*, vol. 44, no. 2, pp. 105–114, Feb. 1997.

[6] N. Memon, X. Kong, and J. Cinkler, "Context-based lossless and near-lossless compression of EEG signals," *IEEE Trans. Biomed. Eng.*, vol. 3, no. 3, pp. 231–238, Mar. 1999.

[7] N.Sriraam and C.Eswaran, "Performance evaluation of neural network and linear predictors for near-lossless compression of EEG signals," *IEEE Trans. Inf. Technol. Biomed.*, vol. 12, no. 1, pp. 87–93, Jan. 2008.

[8] Z. Sijerčić and G. Agarwal, "Tree structured filter bank for time-frequency decomposition of EEG signals," in *IEEE 17th Annual Conf. EMBS*, vol. 2, sep. 1995, pp. 991–992.

[9] V. Kavitha and D. Narayana Dutt, "Use of chaotic modeling for transmission of EEG data," in *Intl Conf. on Inf., Commun. and Signal Process. (ICICS)*, vol. 3, sep. 1997, pp. 1262–1265.

[10] J. L. Cárdenas-Barrera, J. V. Lorenzo-Ginori, and E. Rodríguez-Valdivia, "A wavelet-packet based algorithm for EEG signal compression," *Infor-matics for Health and Social Care*, vol. 29, no. 1, pp. 15–27, 2004.

[11] S. K. Mitra and S. N. Sarbhadhikari, "Iterative system function and genetic algorithm based EEG compression," *Med. Eng. & Physics*, vol. 19, no. 7, pp. 605–617, 1997.

[12] H. Gürkan, U. Guz, and B. S. Yarman, "EEG signal compression based on classified signature and envelope vector sets," *Intl J. Circuit theory and Appl.*, vol. 37, no. 2, pp. 351–363, 2009.

[13] K.-K. Poh and P. Marziliano, "Compressive sampling of EEG signals with finite rate of innovation," *EURASIP J. Advances in Signal Process.*, vol. 2010, pp. 1–12, 2010.

[14] Y. Wongsawat, S. Oraintara, T. Tanaka, and K. Rao, "Lossless multi-channel EEG compression," in *Proc. IEEE Intl Symp. on Circuits and Syst. (ISCAS)*, sep. 2006, pp. 1611–1614.

[15] D. Gopikrishna and A. Makur, "A high performance scheme for EEG compression using a multichannel model," in *High Perf. Computing HiPC 2002*, ser. LNCS, vol. 2552. Springer Berlin / Heidelberg, 2002, pp. 443–451.

[16] Q. Liu, M. Sun, and R. Sclabassi, "Decorrelation of multichannel EEG based on hjorth filter and graph theory," in *6th Intl Conf. on Signal Process.*, vol. 2, Aug. 2002, pp. 1516–1519.

[17] K. Srinivasan and M. R. Reddy, "Efficient pre-processing technique for lossless real-time EEG compression," *Electronics Letters*, vol. 46, no. 1, pp. 26–27, Jan. 2010.

[18] S. Yea and W. Pearlman, "A wavelet-based two-stage near-lossless coder," *IEEE Trans. Image Process.*, vol. 15, no. 11, pp. 3488–3500, Nov. 2006.

[19] W. A. Pearlman and A. Said, "Set partition coding: Part I of set partition coding and image wavelet coding systems," *Foundations and trends in signal process.*, vol. 2, no. 2, pp. 95–180, 2008.

[20] W. A. Pearlman, A. Islam, N. Nagaraj, and A. Said, "Efficient, low-complexity image coding with a set-partitioning embedded block coder," *IEEE Trans. Circuits Syst. Video Technol.*, vol. 14, no. 11, pp. 1219 – 1235, Nov. 2004.

[21] X. Tang, W. A. Pearlman, and J. W. Modestino, "Hyperspectral image compression using three-dimensional wavelet coding," in *Image and Video Commun. and Process.*, ser. Proc. of the SPIE, vol. 5022, 2003, pp. 1037–1047.

[22] J. E. Fowler, "Shape-adaptive coding using binary set splitting with k-d trees," in *Intl Conf. on Image Process.*, vol. 2, Singapore, 2004, pp. 1301 – 1304.

[23] J. T. Rucker and J. E. Fowler, "Coding of ocean-temperature volumes using binary set splitting with k-d trees," in *Intl Geoscience and Remote Sensing Symp.*, 2004, pp. 289 – 292.

[24] A. Said, *Lossless compression Handbook*. Academic Press, 2003, ch. Arithmetic Coding.

[25] ——, "On the reduction of entropy coding complexity via symbol grouping: I redundancy analysis and optimal alphabet partition," HP Labs Palo Alto, Tech. Rep. HPL-2004-145, 2004.

[26] A. L. Goldberger, L. A. N. Amaral, L. Glass, J. M. Hausdorff, P. C. Ivanov, R. G. Mark, J. E. Mietus, G. B. Moody, C.-K. Peng, and H. E. Stanley, "PhysioBank, PhysioToolkit, and PhysioNet : Components of a New Research Resource for Complex Physiologic Signals," *Circulation*, vol. 101, no. 23, pp. e215–220, 2000.

[27] G. Schalk, D. J. McFarland, T. Hinterberger, N. Birbaumer, and J. R.Wolpaw, "BCI2000: A general-purpose brain-computer interface (BCI) system," *IEEE Trans. Biomed. Eng.*, vol. 51, no. 6, pp. 1034–1043, June 2004.

[28] G. Dornhege, B. Blankertz, G. Curio, and K.-R. Müller, "Boosting bit rates in non-invasive EEG single-trial classifications by feature combination and multi-class paradigms," *IEEE Trans. Biomed. Eng.*, vol. 51, no. 6, pp. 993 – 1002, June 2004.

[29] B. Blankertz, G. Dornhege, M. Krauledat, K.-R. Müller, and G. Curio, "The non-invasive berlin brain-computer interface: Fast acquisition of effective performance in untrained subjects," *NeuroImage*, vol. 37, no. 2, pp. 539 – 550, 2007.

[30] J. E. Fowler, "QccPack: An open-source software library for quantiza-tion, compression and coding," in *Appl. of Digital Image Process. XXIII*, ser. Proc. SPIE 4115, 2000, pp. 294–301.